

A modular microscale granuloma model for immune-microenvironment signaling studies *in vitro*

Samuel B. Berry¹, Maia S. Gower¹, Xiaojing Su¹, Chetan Seshadri², Ashleigh B. Theberge^{1,3*}

¹Department of Chemistry, University of Washington, Seattle, WA USA

²Department of Medicine, University of Washington, Seattle, WA USA

³Department of Urology, University of Washington, Seattle, WA USA

*correspondence:

Dr. Ashleigh Theberge

Abt1@uw.edu

Keywords: *in vitro* granuloma model, open microfluidics, immune signaling

Abstract:

Tuberculosis (TB) is one of the most potent infectious diseases in the world, causing more deaths than any other single infectious agent. TB infection is caused by inhalation of *Mycobacterium tuberculosis* (Mtb) and subsequent phagocytosis and migration into the lung tissue by innate immune cells (e.g., alveolar macrophages, neutrophils, dendritic cells), resulting in the formation of a fused mass of immune cells known as the granuloma. Considered the pathological hallmark of TB, the granuloma is a complex microenvironment that is crucial for pathogen containment as well as pathogen survival. Disruption of the delicate granuloma microenvironment *via* numerous stimuli, such as variations in cytokine secretions, nutrient availability, and the makeup of immune cell population, can lead to an active infection. Herein, we present a novel *in vitro* model to examine the soluble factor signaling between a mycobacterial infection and its surrounding environment. Adapting a newly developed suspended microfluidic platform, known as Stacks, we established a modular microscale infection model containing human immune cells and a model mycobacterial strain that can easily integrate with different microenvironmental cues through simple spatial and temporal “stacking” of each module of the platform. We validate the establishment of suspended microscale (4 μ L) infection cultures that secrete increased levels of proinflammatory factors IL-6, VEGF, and TNF α upon infection and form 3D aggregates (granuloma model) encapsulating the mycobacteria. As a proof of concept to demonstrate the capability of our platform to examine soluble factor signaling, we cocultured an *in vitro* angiogenesis model with the granuloma model and quantified morphology changes in endothelial structures as a result of culture conditions ($P < 0.05$ when comparing infected vs. uninfected coculture systems). We envision our modular *in vitro* granuloma model can be further expanded and adapted for studies focusing on the complex interplay between granulomatous structures and their surrounding microenvironment, as well as a complementary tool to augment *in vivo* signaling and mechanistic studies.

1 **Introduction:**

2 Tuberculosis (TB) is one of the most potent infectious diseases in the world, causing
3 more deaths than any other single infectious agent.(World Health Organization 2019) TB
4 infection is caused by inhalation of *Mycobacterium tuberculosis* (Mtb) and subsequent
5 phagocytosis and migration into underlying lung tissue and the lymph system by responding
6 immune cells (e.g., alveolar macrophages, dendritic cells).(Saunders and Britton 2007;
7 Kaufmann 2004) Due to the inability of these innate immune cells to clear Mtb, persistent Mtb
8 induce an adaptive immune response, leading to the formulation of a fused mass of immune cells
9 around Mtb known as a granuloma.(Saunders and Britton 2007) Within the granuloma, Mtb
10 typically enter a latent phase characterized by a non-proliferative phenotype and lipid
11 uptake(Russell et al. 2009; Peyron et al. 2008; Deb et al. 2009), leading to a latent infection that
12 is effectively contained.(World Health Organization 2019) However, disruption of the delicate
13 equilibrium between proinflammatory factors (e.g., tumor necrosis factor- α (TNF α), interferon- γ
14 (IFN γ)), microenvironment conditions (e.g., hypoxia, pH), and immune cell populations (e.g.,
15 macrophages, T cells) can lead to reactivation of latent Mtb and deterioration of the granuloma,
16 initiating an active TB infection and dissemination of infectious mycobacteria.(Russell et al.
17 2009; Ramakrishnan 2012)

18 Deciphering the impact of microenvironment variations around the granuloma remains a
19 significant challenge, and researchers often rely on *in vivo* animal models or biological samples
20 (e.g., blood, tissue biopsy), considered the gold standard for studying TB, to reconstruct this
21 complex environment. These methods have laid the foundation for understanding the
22 pathogenesis and immunology behind TB, yet many existing *in vivo* models do not accurately
23 recapitulate Mtb infection as seen in humans (although recent advances in mouse models and the
24 established zebrafish/*M. marinum* model are closing this gap)(Cronan et al. 2018; Myllymäki,
25 Bäuerlein, and Rämetsä 2016; Gern et al. 2017; Cronan and Tobin 2014; Zhan et al. 2017; Yong,
26 Her, and Chen 2018). Additionally, despite recreating the complexity of an *in vivo* environment,
27 spatial manipulation and probing of the granuloma microenvironment through introduction or
28 removal of immune and tissue components is difficult in most animal models.(Scanga and Flynn
29 2014; Foreman et al. 2017; Zhan et al. 2017) Further, human-derived biological samples provide
30 detailed cellular information regarding the granuloma, the immune response, and disease status
31 (Darboe et al. 2019; Guyot-Revol et al. 2006; Ogongo et al. 2020; Berry et al. 2010), but are
32 inherently limited as they only reflect a singular point in time, rather than the dynamic
33 interactions that occur during the early stages of infection or disease progression.

34 Alternatively, researchers have utilized *in vitro* models to examine specific processes and
35 immune phenomena associated with TB infection and granuloma formation, augmenting the
36 valuable information elucidated from *in vivo* models.(Peyron et al. 2008; Deb et al. 2009;
37 Birkness et al. 2007; Kapoor et al. 2013; Elkington et al. 2019) These models, which often rely
38 on infection of patient-derived peripheral blood mononuclear cells (PBMCs) with mycobacterial
39 strains, have successfully mimicked granuloma formation and behavior through soluble factor
40 signaling between immune cells (Birkness et al. 2007; Puissegur et al. 2004; Crouser et al. 2017),
41 Mtb reactivation(Kapoor et al. 2013), and PBMC differentiation.(Peyron et al. 2008) However,
42 many of these *in vitro* models consist of granulomas grown inside of well plates(Peyron et al.
43 2008; Birkness et al. 2007; Kapoor et al. 2013; Puissegur et al. 2004; Crouser et al. 2017),

1 limiting the ability of the researchers to easily manipulate the microenvironment of the
2 granulomas and increase the complexity of their granuloma models through multiculture and
3 introduction of key components of the microenvironment on demand. Recently, more complex,
4 biomimetic models have been developed that have successfully recapitulated important
5 biological phenomena(Venkata Ramanarao Parasa et al. 2014; Venkata R. Parasa et al. 2017) and
6 examined novel therapeutic approaches to combat TB infection (Tezera et al. 2017; Bielecka et
7 al. 2017), while simultaneously demonstrating innovative and tractable platforms. However,
8 these models face limitations in studies where users wish to subject granulomas to various
9 microenvironmental cues over time, or in enabling the addition of tissue components after the
10 model is established.

11 Building upon the foundation created by previous *in vitro* models, we present the creation
12 of a novel microscale *in vitro* granuloma model that can be adapted to study the soluble factor
13 signaling between granulomas and their surrounding microenvironment immediately following
14 infection. Using a recently developed modular microfluidic coculture platform, known as
15 “Stacks”(Yu et al. 2019), we demonstrate a multi-layered coculture that can be spatially and
16 temporally manipulated to mimic different microenvironments and timepoints. The Stacks
17 platform utilizes suspended cultures, wherein a droplet is contained in a well consisting of walls
18 but lacking a ceiling or floor (Casavant et al. 2013; Humayun, Chow, and Young 2018; Berthier
19 et al. 2019), thereby enabling users to vertically stack layers containing different cell types and
20 place them in signaling contact.(Yu et al. 2019) The modular component of the Stacks, as well as
21 of other microfluidic platforms, offers a notable advantage as users can optimize model
22 conditions individually and connect each component to create different complex systems.(Yu et
23 al. 2019; Ong et al. 2019) As a proof of concept, we use a model mycobacterial strain known to
24 induce granuloma formation *in vitro*(Puissegur et al. 2004; Seitzer and Gerdes 2003),
25 *Mycobacterium bovis* Bacillus Calmette-Guerin (BCG), with human blood-derived immune cells
26 and validate its ability to form an *in vitro* granuloma model on the microscale (4 μ L culture
27 volume) in a layer of the Stacks platform. Further, to demonstrate the ability of our stackable
28 microscale infection model to signal with its surrounding microenvironment, we miniaturize an
29 existing *in vitro* angiogenesis model (containing primary human endothelial cells) within a
30 separate stackable layer.(Yu et al. 2019; Koh et al. 2008; Lonza 2018) Here, we validate the
31 development of our microscale *in vitro* granuloma model and demonstrate the capability of the
32 system to support soluble factor signaling between the granuloma model and a separate stackable
33 endothelial culture. We envision our modular *in vitro* granuloma model can be further developed
34 to include additional layers of immune cells, tissue models, and pathogens for studies examining
35 the complex interplay between granulomatous structures and their surrounding environment, as
36 well as a complementary tool to augment *in vivo* signaling and mechanistic studies.

37

38 **Results and Discussion:**

39

40 *Microscale Granuloma Model Design and Overview*

41 We present a modular *in vitro* platform that we adapted to enable the ability to add,
42 modify, and manipulate the granuloma microenvironment for studying the effects of cellular
43 signaling on granuloma formation and development. To create this *in vitro* model, we adapted a

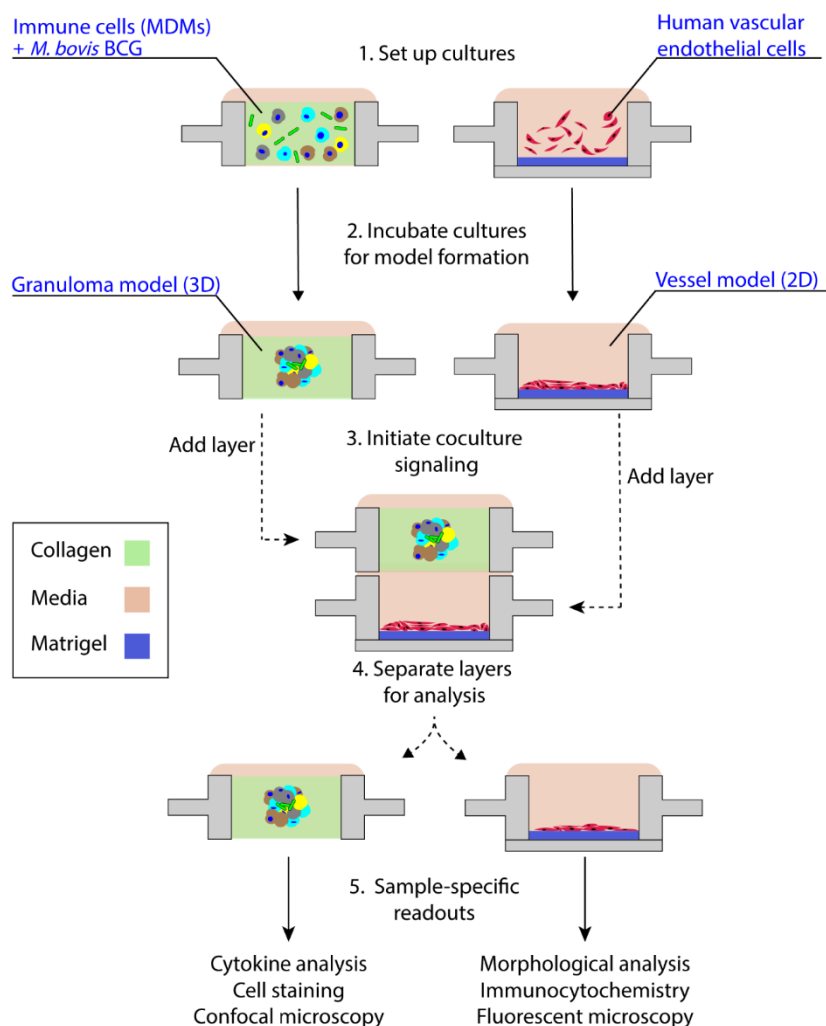
1 previously described open microfluidic platform (“Stacks”(Yu et al. 2019)) (Figure 1) that relies
2 on key fluidic principles, namely capillary pinning, to enable vertical stacking and removal of
3 discrete cell culture wells without leakage or horizontal flow between stacked layers. The
4 pinning of fluids within this platform is vital to contain cultures within the open wells and allows
5 for the connection and separation of the wells without bonding or disruption of the cultures,
6 respectively. Additionally, the Stacks platform provides numerous advantages such as pipette
7 accessibility (due to its open culture wells), bio- and imaging compatibility (due to its fabrication
8 from polystyrene or polypropylene), and microscale culture wells. Further, the Stacks device
9 relies on surface tension and capillary forces for functionality, removing the need for external
10 pumps commonly associated with microfluidic chips (i.e., syringe pumps) and allowing it to fit
11 within common cell culture materials (e.g., OmniTray™, petri dish) and incubators. For our *in*
12 *vitro* model, we created two independent layers that can be clicked together to initiate paracrine
13 signaling or separated for independent analysis, thereby allowing us to temporally introduce
14 different signaling microenvironments to our *in vitro* granuloma model (Figure 1).(Yu et al.
15 2019) The first layer, herein called the granuloma layer, consists of an infection model of
16 monocyte-derived macrophages (MDMs) and a model mycobacterium strain, *Mycobacterium*
17 *bovis* Bacillus Calmette-Guérin (BCG), suspended in a 3D extracellular matrix (ECM) plug to
18 mimic some aspects of *in vivo* granuloma behavior (e.g., pathogen encapsulation, soluble factor
19 secretion, aggregate formation) previously observed in other *in vitro* granuloma
20 models.(Birkness et al. 2007; Kapoor et al. 2013; Crouser et al. 2017) The second layer, herein
21 called the endothelial layer, consists of an *in vitro* angiogenesis model in which endothelial cells
22 are cultured on a hydrogel plug. By placing the primary human endothelial cells on a separate
23 Stacks layer, our model can be used to examine the induction of angiogenic processes around the
24 granuloma layer and how those angiogenic processes are affected by the soluble factor signaling
25 profile of the granuloma layer. It is important to note that in our platform, the granuloma layer is
26 not vascularized directly, as is observed *in vivo*(Datta et al. 2015), and that in our system, our
27 endothelial layer is more akin to modeling the surrounding vasculature that is manipulated
28 during early TB infection (Figure 1).(Polena et al. 2016)

29 Previous *in vitro* granuloma models successfully recapitulated important components of
30 granulomatous infections including leukocyte recruitment and signaling, establishment of
31 dormancy and resuscitation, and genetic diversity at scales ranging from 12 well plates to 96 well
32 plates.(Birkness et al. 2007; Crouser et al. 2017; Kapoor et al. 2013) Our model adds to these
33 existing techniques through miniaturization and introduction of modularity to enable
34 examination of the signaling phenomena between a mycobacterial infection and its surrounding
35 microenvironment. We reduce the volume of our cultures (4 μ L/well) more than 10-fold from
36 previous examples (50-500 μ L/well) to decrease cell and reagent usage in our model; further, we
37 mix BCG and MDMs together in a 3D extracellular matrix (ECM), without pre-infecting the
38 MDMs, to establish the infection in our granuloma layer after a minimum of 24 hours (Figure 1).
39 However, due to the scale of the model (4 μ L/well), the media buffering capacity, nutrient
40 availability, waste accumulation, and multiplicity of infection (MOI) all needed to be optimized
41 to permit successful formation of the granuloma layer (Supplementary Information 2). This is
42 consistent with prior investigations on the effects of miniaturization on mammalian cultures.(Su
43 et al. 2013) Similarly, we adapted and miniaturized the established *in vitro* angiogenesis

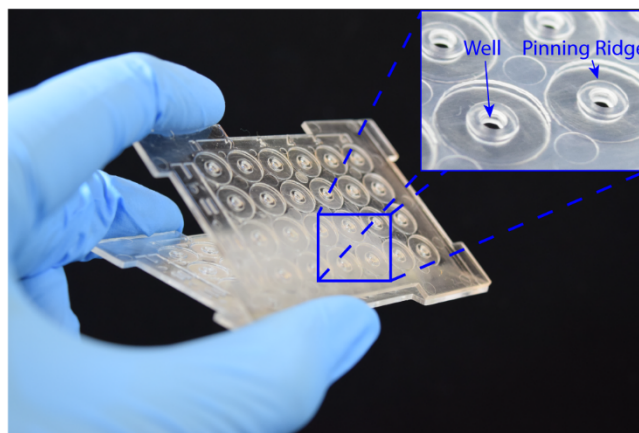
1 assay(Lonza 2018; Koh et al. 2008) that is seeded into a separate Stacks layer and subsequently
2 clicked together with the granuloma layer to initiate soluble factor signaling between the two
3 layers (Figure 1, 4, Supplementary Information 3).

4

A) Cross-Sectional Schematic Workflow



B) Modular Suspended Microfluidic Platform: "Stacks"



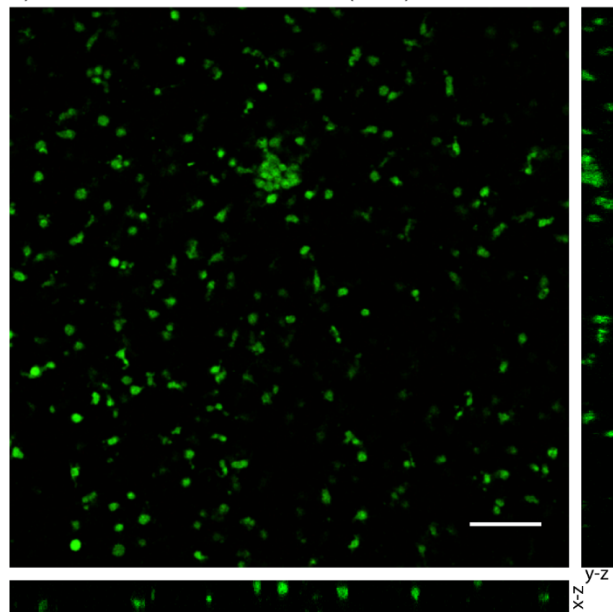
1
2 **Figure 1:** Suspended open microfluidic platform enables creation of a modular *in vitro*
3 granuloma model. A) Schematic workflow showing cross sections of establishing the granuloma
4 and endothelial layers and stacking of layers to initiate coculture paracrine signaling. B) The

1 “Stacks” platform(Yu et al. 2019) contains an array of 24 individual suspended wells to facilitate
2 the exchange of signals through the top and bottom of the well to neighboring layers and can be
3 easily combined and removed. The inset illustrates the open suspended wells (2 mm diameter)
4 and pinning ridges required to prevent leakage within the platform.
5

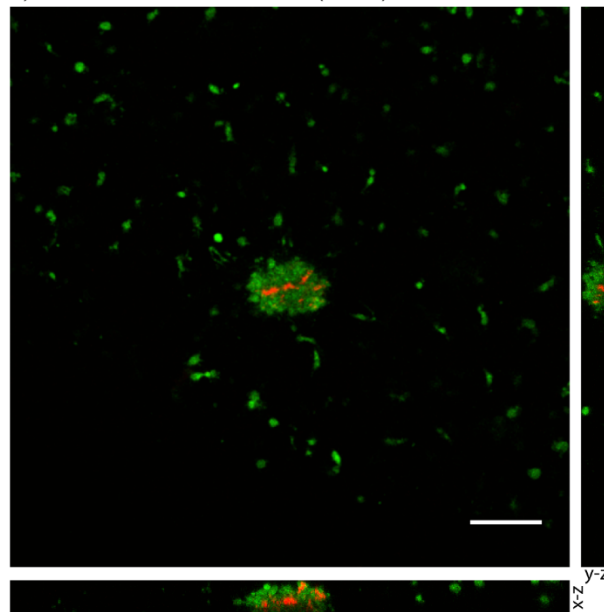
6 *Validation of Granuloma Model in Stacks Platform*

7 To validate the successful establishment of a microscale *in vitro* granuloma model within
8 our platform, we used three separate previously reported readouts: 1) aggregate formation, 2)
9 encapsulation of the mycobacterium within host immune cells, and 3) soluble factor
10 analysis.(Birkness et al. 2007; Kapoor et al. 2013; Crouser et al. 2017; Tezera et al. 2017) After
11 initiating infection by mixing MDMs and BCG into the ECM (collagen I) and seeding it into the
12 wells, we consistently observed aggregate formation in the granuloma layer containing BCG
13 when wells were fixed and imaged on Day 4 post infection (p.i.) (Figure 2). Using mCherry-
14 expressing BCG, we were able to observe aggregation of CellTracker Green-stained MDMs
15 around the BCG in infection wells, whereas little to no aggregate formation was observed in the
16 uninfected control wells (Figure 2); the 3D structure of the aggregates containing MDMs and
17 BCG was confirmed through confocal imaging of the granuloma layers on Day 4 p.i. (Figure 2).
18 We observed complete encapsulation of BCG within the multi-cellular aggregate, oftentimes
19 noting the presence of multiple spatially distinct BCG within one aggregate and little to no
20 extracellular BCG (Figure 2). An advantage of mixing the BCG and MDMs without direct pre-
21 infection of the MDMs is that MDMs must sample and migrate through the 3D collagen matrix
22 in order to initiate the infection and respond to other infected MDMs, a process which is further
23 supported by the microscale culture wells and an optimized MOI of 0.05.

A) Uninfected Granuloma Model (-BCG)



B) Infected Granuloma Model (+BCG)

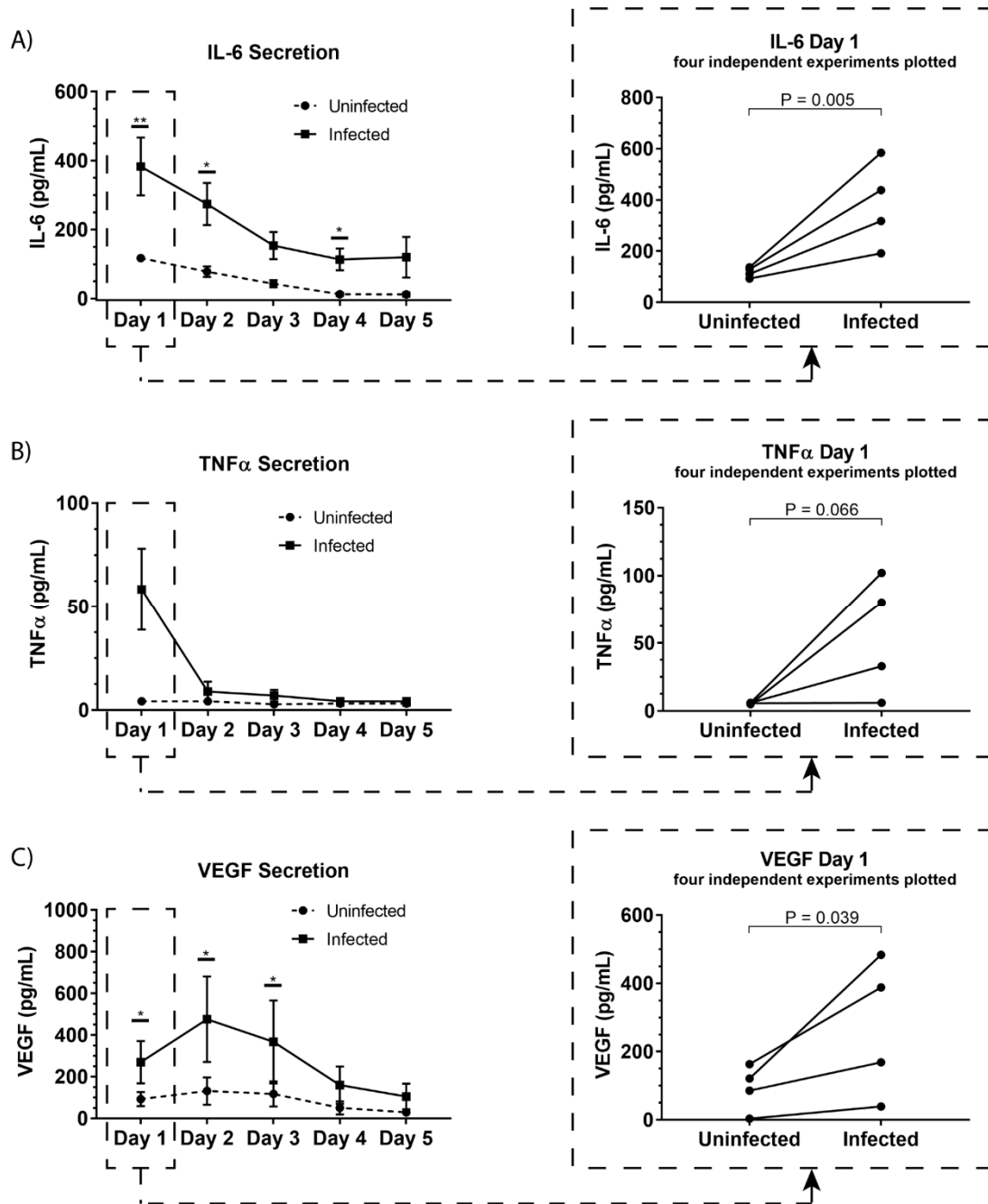


24

25 Figure 2: Aggregation of *M. bovis* BCG and MDMs in 3D collagen plugs within a layer of the
26 Stacks microscale culture system. A) CellTracker Green-stained MDMs remain dispersed in a

1 3D collagen plug in the absence of coincubation with BCG. B) MDMs encapsulate mCherry-
2 expressing BCG in the granuloma layer and form large multicellular aggregates that surround the
3 BCG-infected MDMs and contain the mycobacterium within the aggregate. Confocal
4 microscopy shows the structure of the aggregated MDMs with BCG and illustrates containment
5 of the BCG within the aggregate of MDMs in the suspended 3D collagen plug. Representative
6 images obtained on Day 4 p.i. MOI: 0.05. Scale bar: 100 μm . Bottom image depicts x-z plane
7 (66.5 μm thickness) and right image depicts y-z plane (66.5 μm thickness).

8 To illustrate the capability of our model to be used for soluble factor signaling studies, we
9 analyzed the secretion profile of three granuloma-associated proinflammatory factors:
10 interleukin-6 (IL-6), tumor necrosis factor α (TNF α), and vascular endothelial growth factor
11 (VEGF) (Figure 3). (Polena et al. 2016; Martinez, Mehra, and Kaushal 2013; Lin et al. 2007;
12 Singh and Goyal 2013) In accordance with previous models and studies (Birkness et al. 2007;
13 Polena et al. 2016; Martinez, Mehra, and Kaushal 2013; Singh and Goyal 2013; Lin et al. 2007)
14 we observed significantly greater secretion of IL-6 ($P = 0.005$) and VEGF ($P = 0.039$) in our
15 infected granuloma layers (+BCG) when compared to our control layers containing uninfected
16 MDMs in monoculture (-BCG); further, we observed a 5-17-fold increase in TNF α secretion in 3
17 out of 4 independent experiments under the same conditions and a strong trend towards greater
18 TNF α secretion (Figure 3). We also observed decreasing secretion of IL-6, TNF α , and VEGF
19 over 5 days, with the greatest concentrations observed for IL-6 and TNF α on Day 1 and for
20 VEGF on Day 2 (Figure 3). These results indicate that there is a large burst of proinflammatory
21 factors immediately following infection, that then decreases and stabilizes over time as we begin
22 to observe aggregate formation in the granuloma layers. Additionally, while we observe the
23 anticipated increases in the secretion of these factors, we would expect a more robust response if
24 more virulent strains than BCG were used, as increased secretion of factors has been observed
25 with infection by more virulent mycobacterial strains. (Engele et al. 2002; Polena et al. 2016)
26 Thus, these results support the use of our microscale granuloma model for studies of soluble
27 factor signaling involving the granuloma layer, and its broader use for mycobacterial infection
28 cytokine studies. (Domingo-Gonzalez et al. 2016)



1
2 **Figure 3:** Soluble factor analysis of granuloma layer supernatants illustrates proinflammatory
3 profile of infection model. Infection with BCG causes significant increases in secretion of (A)
4 IL-6 and (C) VEGF in the Stacks platform, and shows an increasing trend in (B) TNF α secretion
5 Day 1 p.i. Secretion of IL-6, TNF α , and VEGF decreases over time in infected granuloma layers
6 following infection, corresponding with the formation of aggregates starting around Day 3 p.i.
7 For Day 1-5 p.i., media was replaced daily and supernatant collected from each day was
8 analyzed. Each point represents pooled supernatant samples from 24 technical replicates from
9 n=4 independent experiments (each of the four independent experiments is plotted as a separate

1 point in the plots on the right for the Day 1 data). Error bars on left plot: SEM. *P < 0.05; **P <
2 0.01; Ratio paired *t*-test.

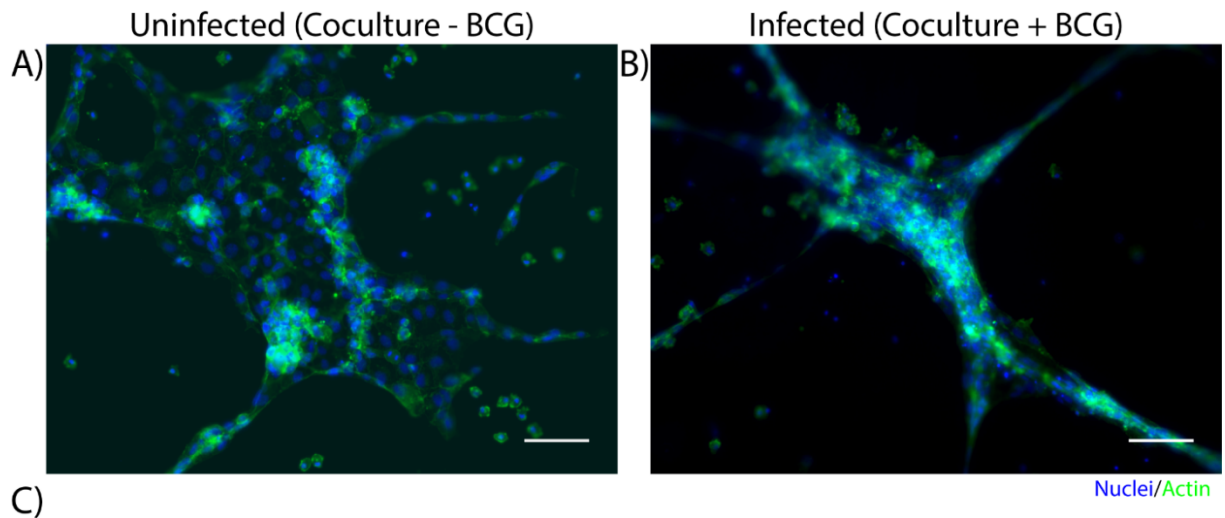
3 *BCG Granulomas Modulate Endothelial Structure Morphology In Vitro*

4 As a proof of concept to demonstrate the use of our microscale granuloma model in the
5 Stacks platform, we developed a coculture system containing an established angiogenesis
6 model(Theberge et al. 2015b; Yu et al. 2019; Lonza 2018; Koh et al. 2008; Sarkanen et al. 2011)
7 that can be used to probe granuloma-associated angiogenesis.(Osherov and Ben-Ami 2016;
8 Polena et al. 2016; Oehlers et al. 2015; Datta et al. 2015) Mycobacterium-mediated angiogenic
9 processes and granuloma vascularization result from the secretion of proangiogenic factors by
10 the infected immune cells that compose the granuloma and play a complex and evolving role
11 during the course of infection.(Torraca et al. 2017; Polena et al. 2016; Oehlers et al. 2015; 2017)
12 Extensive work has been conducted on understanding the role of angiogenesis in granuloma
13 outcome, finding that inhibition of VEGF and other signaling pathways reduces pathogenicity
14 and dissemination of infectious mycobacteria(Polena et al. 2016; Oehlers et al. 2015; Harding et
15 al. 2019) while normalizing surrounding vasculature, improving small molecule delivery, and
16 decreasing hypoxia within the granuloma.(Datta et al. 2015) Similarly, we observed increased
17 secretion of VEGF from infected cells within our microscale granuloma model (Figure 3C), and
18 therefore sought to illustrate one potential use of our platform as a complimentary tool for
19 studies examining this infection-mediated process.

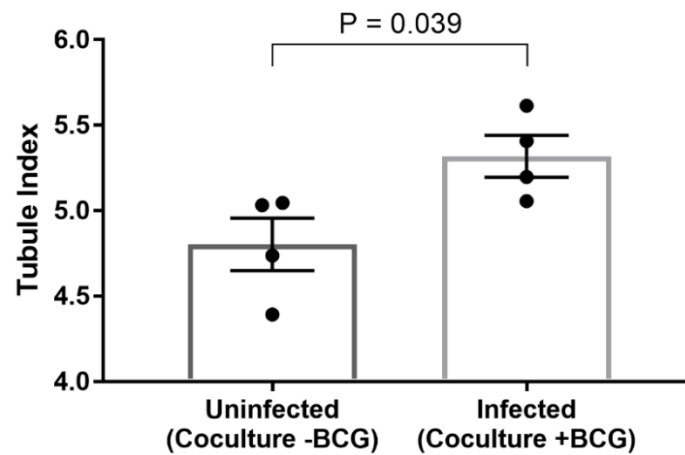
20 To establish this granuloma-vasculature model coculture system, we created a second
21 Stacks layer containing a floor, enabling culture of human endothelial cells on a hydrogel plug
22 (Matrigel) while retaining the ability to be placed in soluble factor signaling contact with the
23 granuloma layer. We selected an *in vitro* model of angiogenesis that has been extensively used to
24 screen angiogenic stimulants and inhibitors, wherein human endothelial cells cultured in well
25 plates self-assemble into tubule-like networks and demonstrate cell sprouting and branching, and
26 adapted it for our endothelial layer.(Bishop et al. 1999; Lonza 2018; Koh et al. 2008; Sarkanen et
27 al. 2011) In order to examine the influence of the soluble factor profile from the granuloma layer
28 on the endothelial layer, we independently established the granuloma layer and the endothelial
29 layer under their optimized culture conditions; the modularity of the Stacks platform enables
30 both layers to be cultured in their optimal conditions (and in separate incubators) without risk of
31 cross contamination prior to joining the layers. The granuloma layers were infected and
32 incubated 24 hours prior to clicking with the endothelial layer, and the endothelial layers were
33 seeded 2 hours prior to allow the cells to self-assemble into a tubule-like network.(Lonza 2018;
34 Sarkanen et al. 2011) Separate layers were then stacked together and connected by a bridge of
35 shared media to allow passage of factors between the two layers. After 16 hours of signaling, we
36 separated the layers and fixed, stained, and imaged the vasculature to analyze its morphology as
37 a result of coculture with the granuloma layer (Figure 4). We found that after 16 hours of
38 coculture, endothelial cells in contact with infected granuloma layers (+BCG) formed thinner,
39 centralized structures with diffuse cell sprouts extending from the center, whereas endothelial
40 cells in contact with uninfected control layers (-BCG) formed wider and larger structures that
41 retained some interconnected networks (Figure 4). We quantified these morphological
42 differences through measurement of their tubule index, a metric that measures the ratio of the

1 endothelial structure perimeter to the endothelial structure area and can be used to discern
2 between endothelial structure morphologies (e.g., tubule network, single tubule,
3 islands/clusters)(Theberge et al. 2015a), and found significant morphological differences
4 between endothelial layers cocultured with infected granuloma layers (+BCG) when compared
5 uninfected granuloma layers (-BCG) (Figure 4). The morphological change is likely the result of
6 the increased secretion of factors from BCG-infected MDMs, such as VEGF (Figure 3C);
7 however, it is possible that additional factors we did not quantify are also contributing to the
8 differences in endothelial morphology. Ultimately, the induction of morphology changes in the
9 endothelial layer as a result of coculture with different model granuloma layers illustrates the
10 ability of the granuloma layer to signal with a neighboring layer representing
11 microenvironmental components.

12 As we chose to connect the layers at Day 1 p.i. to correlate with increased levels of
13 VEGF and cytokine secretion (Figure 3), we expect our model and results would mimic an
14 earlier time point in infection, when the mycobacteria-infected cells are still secreting
15 proinflammatory factors to recruit other immune cells and the vasculature. Depending on user
16 queries, these layers can also be stacked at more advanced time points to study the effect of a
17 later soluble factor profile on the surrounding vasculature, illustrating a key advantage of the
18 modularity of the Stacks system and the flexibility in timing to combine the layers. Further, the
19 ability of the model granuloma layer to communicate with the vasculature and modulate the
20 endothelial morphology demonstrates the usage of this platform for signaling studies between
21 our infected granuloma layers and microenvironment components. The ability to create two
22 independent layers that are in soluble factor signaling contact enables users to isolate the effects
23 of the soluble factors from the granuloma layer on its surrounding microenvironment without
24 interference from juxtacrine signaling or physical interactions.



Morphology of Multicellular Endothelial Structures



1

2 **Figure 4:** Coculture of endothelial layer with granuloma layer impacts morphology of
3 multicellular endothelial structures. Representative images of an endothelial layer cocultured
4 with an uninfected (-BCG) layer (A) or infected (+BCG) layer (B) for 16 hours, illustrating the
5 difference in endothelial morphology as a result of coculture. C) The tubule index
6 (perimeter/area ratio) was used to quantify the morphology of endothelial structures and shows a
7 significant difference between coculture conditions, demonstrating the ability of the model
8 granuloma layer to signal with the endothelial layer. Scale bar: 100 μ m. Error bars: SEM. $P <$
9 0.05, unpaired t -test. Each point represents the average ratio of an independent experiment (n=4
10 independent experiments are plotted).

11 **Conclusion:**

12 Microenvironmental effects, such as soluble factor signaling, play a vital role in
13 granuloma outcome, as the immune system attempts to contain and impede pathogenic
14 mycobacterium from manipulating its environment in favor of its survival.(Ramakrishnan 2012)
15 For example, induction of angiogenic processes by Mtb in the microenvironment surrounding a
16 granuloma have been linked to pro-pathogen outcomes(Osherov and Ben-Ami 2016; Oehlers et

1 al. 2015), while treatment with anti-angiogenic factors can be a potential treatment option to
2 improve the effects of existing drug regimens.(Datta et al. 2015) To further understand the
3 signaling environment and timeline of these phenomena, we created a novel *in vitro* granuloma
4 model that can be used to study soluble factor signaling between the granuloma and its
5 surrounding microenvironment. As a proof of concept model, we created a two-layered modular
6 microfluidic system containing a mycobacterial infection and an endothelial vasculature model
7 that can be used to compliment *in vivo* granuloma and angiogenesis models.(Polena et al. 2016;
8 Oehlers et al. 2015; 2017; Datta et al. 2015) We demonstrate creation of a viable mycobacterial
9 infection using human blood-derived immune cells and BCG within a 4 μ L suspended collagen
10 plug, and validate the secretion of proinflammatory cytokines associated with mycobacterial
11 infection. Further, we provide a model coculture system that can be used to probe granuloma-
12 associated angiogenic processes *in vitro*. The modularity and microscale size of our model
13 enables users to add or remove additional cell types at various time points, and to utilize limited
14 cell populations, such as patient cells or rare immune cells, and valuable reagents, such as
15 antibodies or expensive drugs. Additionally, the design of the platform and fabrication method
16 supports the creation of arrays to test various culture conditions/treatments and customizability to
17 introduce additional functionality (e.g., flow), as well as easy integration with BSL3 laboratory
18 workflows as the device is disposable and fits inside common cell culture materials (e.g., petri
19 dish, OmniTray™, etc.). Further development of our system includes the addition of adaptive
20 immune cells (e.g., T cells) and introduction of parenchymal and stromal cells (e.g., epithelial
21 cells, fibroblasts) to model signaling interactions in the pulmonary environment, as well as the
22 use of virulent *M. tuberculosis* to induce more *in vivo*-like responses. Ultimately, we created a
23 tractable and customizable mycobacterial infection model that can be utilized by other
24 researchers to examine the various signaling components of a complex tuberculosis infection.

25 26 **Materials and Methods:**

27 *Stacks Device Fabrication:*

28 Stacks devices(Yu et al. 2019) were fabricated from either polypropylene (PP)
29 (granuloma layer) or polystyrene (PS)(endothelial layer)(Supplementary Figure 1, Table 1). PP
30 devices were injection molded (ProtoLabs, Maple Plain, MN, USA) and were flattened using a
31 bench top manual heated press (#4386, Carver Inc., Wabash, IN) for 1 h at 110°C (protocol in
32 Supplementary Information 1). After flattening, devices were cleaned with isopropanol (IPA)
33 sonication for 1 h to remove any fabrication residue or contaminants, and then rinsed twice with
34 fresh IPA before drying with compressed air. Prior to use, devices were UV-sterilized for 30 min
35 in a biosafety cabinet. PS devices containing a floor were designed using Fusion360 CAD
36 software (Autodesk, San Rafael, CA, USA) and milled using a Datron Neo CNC mill (Datron
37 Dynamics Inc., Livermore, CA, USA). PS devices and bottoms (floors, 53 mm x 53 mm) were
38 milled from 1.2 mm thick PS sheets (Goodfellow Corp, Coraopolis, PA, USA). To attach the
39 floor to the PS Stacks layer, floors were solvent bonded to the bottom of the Stacks layer using
40 acetonitrile at 75°C for 10 min, followed by 15 min at 75°C to allow excess acetonitrile to
41 evaporate. Solvent-bonded devices were then sonicated in IPA for 80 min and 70% ethanol for
42 15 min. Devices were then soaked in sterile deionized water for a minimum of 3 hours, dried
43 with compressed air, and UV-sterilized for 30 min prior to use. Device holders were designed on

1 Solidworks CAD software (Solidworks Corp., Waltham, MA, USA), converted into G-code
2 using SprutCAM CAM software (SprutCAM, Naberezhnye Chelny, Russia), and milled using a
3 Tormach PCNC Micromill (Tormach Inc., Waunakee, WI). Device holders were fabricated from
4 4 mm thick PS and were sonicated in IPA for 1 h and UV-sterilized for 30 min prior to use. All
5 device and device holder design files are included in the SI (Supplementary Table 1).

6 To prevent evaporation of microliter volumes of samples, culture platforms were placed
7 in a Nunc Omnitray™ (ThermoFisher) which was then placed in a bioassay dish (#240835,
8 ThermoFisher) for secondary containment; both the Omnitray and bioassay dish were filled with
9 sacrificial water droplets (1 mL and 5 mL, respectively) to create a humidified environment
10 around the platform, and all cultures were then placed into a water-jacketed incubator.

11 12 *Cell Culture:*

13 Human peripheral blood mononuclear cells (PBMCs) were isolated from patient whole
14 blood samples (Bloodworks NW, Seattle, WA, USA) using the Ficoll-Paque PLUS media
15 density separation protocol (ThermoFisher, Waltham, MA, USA). Briefly, blood samples were
16 diluted with PBS (Fisher Scientific) and layered atop the Ficoll-Paque. Tubes were then
17 centrifuged for 20 min at 1900 RPM without brakes, and afterwards white blood cells at the
18 plasma-Ficoll-Paque interface were collected and resuspended in PBS + 2% fetal bovine serum
19 (FBS, ThermoFisher) + 1 mM ethylenediaminetetraacetic acid (EDTA, Gibco, ThermoFisher).
20 Cells were then rinsed with subsequent centrifugation (10 min, 500g) and resuspension until the
21 supernatant was clear. Isolated PBMCs were then cryopreserved in solution containing 90%
22 heat-inactivated FBS (HI-FBS) (ThermoFisher) and 10% dimethyl sulfoxide (DMSO) (Sigma-
23 Aldrich, St. Louis, MO) and stored in liquid nitrogen until use. To differentiate the PBMCs into
24 monocyte-derived macrophages (MDMs), PBMCs were thawed and resuspended in serum free
25 RPMI 1640 media (Gibco, ThermoFisher); following resuspension, PBMCs were seeded into a 6
26 well plate (#3516, Corning Inc., Corning, NY, USA) and allowed to incubate for 3 h at 37°C and
27 5% CO₂ for monocyte adhesion. After 3 h, suspended cells were removed, adherent cells were
28 washed once with 1X phosphate-buffered saline (PBS, Fisher Scientific), and then RPMI 1640
29 containing 10% HI-FBS, 2 mM L-glutamine, 25 mM HEPES, and 50 ng/mL macrophage
30 colony-stimulating factor (M-CSF) (R&D Systems, Minneapolis, MN, USA) was added to each
31 well. Media was changed on Day 3 and Day 6 post-seeding, and MDMs were used after Day 6.

32 mCherry-expressing *M. bovis* Bacillus Calmette-Guérin (BCG) (graciously provided by
33 the Urdahl Lab, Seattle Children's Research Institute, WA, USA) was cultured in Middlebrook
34 7H9 broth (ThermoFisher) containing 10% Middlebrook ADC enrichment supplement
35 (ThermoFisher), 0.003% Tween-80 (Fisher Scientific), and 50 µg/mL hygromycin B (Sigma-
36 Aldrich). A lower Tween-80 concentration had to be used to ensure that the surfactant did not
37 interfere with the microfluidic media pinning in the Stacks device (Supplementary Information
38 2). BCG was cultured at 37°C and 170 RPM to an OD of 0.7-1.0 for use, passed through a 27G
39 needle to break up aggregates, and diluted to a working concentration for the experiment. BCG
40 was used for all experiments as it can be used within a BSL2 facility, and we did not have access
41 to virulent mycobacterium strains nor a BSL3 facility to perform these experiments.

1 Human umbilical vein endothelial cells (HUVECs) (Lonza, Basel, Switzerland) were
2 cultured in completed EGM-2 media and maintained at 37°C and 5% CO₂ until 80-90%
3 confluence. Passage 5-7 cells were used.

4 5 *3D Granuloma Assay:*

6 MDMs were differentiated for a minimum of 6 days prior to use, and BCG was grown to
7 an OD of 0.7-1.0 for use. MDMs were rinsed once with 1X PBS and detached with enzyme-free
8 Cell Dissociation Buffer (#13151014, Life Technologies, ThermoFisher) at 37°C for 5 min and
9 vigorous pipetting. Detached cells were neutralized with complete RPMI 1640 media, counted,
10 and resuspended at a density of 4x10⁷ cell/mL. BCG was vortexed for 30 seconds, vigorously
11 mixed via pipetting, and then diluted into 4 mL of complete RPMI 1640 media for a final
12 concentration of 2x10⁶ BCG/mL. An extracellular matrix (ECM) mix containing 80 µL 3 mg/mL
13 type I bovine collagen (Advanced Biomatrix Inc., Carlsbad, CA, USA), 10 µL 10X HEPES
14 buffer, 7 µL deionized H₂O, 3 µL 0.5N NaOH, and 2.25 µL 1 mg/mL human fibronectin (Sigma-
15 Aldrich) was mixed and stored on ice until use. To prepare the suspended cell-laden collagen
16 plugs, 25 µL of MDMs (at 4x10⁷ cells/mL) and 25 µL of BCG (at 2x10⁶ BCG/mL) or 25 µL of
17 complete RPMI 1640 was added to the ECM mix for a final volume of 152.25 µL and an MOI of
18 0.05. After mixing, 4 µL of the cell-laden ECM mix was added to each well in a PP device and
19 allowed to gel at 37°C and 5% CO₂ for 2 h. After gelation, 8 µL of RPMI 1640 containing 15%
20 HI-FBS and 25 mM HEPES was added atop each well and returned to the incubator. Media was
21 changed daily for the entirety of the experiments. For all monoculture infection experiments
22 (Figures 2 and 3), MDMs were stained with CellTracker Green CMFDA dye (ThermoFisher)
23 according to manufacturer's protocols. Briefly, MDMs were rinsed with 1X PBS, and 10 µM
24 CellTracker Green in serum-free media was added for 30 min at 37°C, washed once with 1X
25 PBS, and then incubated with complete media for 10 min prior to further processing or use.

26 27 *2D Angiogenesis Assay:*

28 Prior to seeding, PS Stacks devices containing a floor were chilled for 5 min at -80°C and
29 then kept on ice for Matrigel seeding. 3µL of Matrigel (8.6 mg/mL) was added to each well and
30 devices rested on ice 30 min. The Matrigel was then polymerized for 30 min at 37°C. After
31 polymerization, 3 µL of HUVECs were added atop the Matrigel for a final concentration of
32 1,650 cells per well (5.5x10⁵ cells/mL). Cells were allowed to adhere and self-assemble for 2 h at
33 37°C and 5% CO₂. Media was then aspirated and replaced with 2 µL of EGM-2 + 10% FBS
34 coculture media.

35 To stack the layers, media was first removed from the model granuloma layers. Model
36 granuloma layers were then placed atop the endothelial layers (containing 3 µL of media) and 7
37 µL of coculture media was placed atop each well of the stacked granuloma layers, to allow for
38 feeding of both layers. Layers were separated by a thin layer of tape along the sides of the
39 devices to ensure reproducible separation. Stacked devices were then placed in the incubator at
40 37°C and 5% CO₂. After 16 h, devices were inverted and separated, fixed with 4%
41 paraformaldehyde for 30 min at 25 °C, and stained as specified under Imaging.

42 43 *Imaging:*

1 To validate granuloma layer formation within our platform, MDMs were prestained with
2 CellTracker Green CMFDA dye prior to infection and seeding into the Stacks. For imaging, the
3 Stacks platform was placed on a 50 mm x 75 mm glass coverslip (#260462, Ted Pella Inc.,
4 Redding, CA, USA) and placed into an OmniTray™ with a 45 mm x 70 mm rectangle cut out of
5 the bottom. Fluorescent images were obtained on a Zeiss Axiovert 200 coupled with an Axiocam
6 503 mono camera (Carl Zeiss AG, Oberkochen, Germany). For confocal imaging, all wells were
7 fixed with 4% paraformaldehyde for 1 h at 25°C and then covered with PBS; the same imaging
8 protocol was then followed as above. Fluorescent confocal images were obtained on a Leica TCS
9 SP5 II Laser Scanning Confocal Microscope (Leica Camera AG, Wetzlar, Germany), with a z-
10 depth of 66.47 µm and step size of 1.01 µm. Images obtained with the Zeiss Axiovert 200 were
11 analyzed with Fiji (ImageJ), and images obtained with the Leica TCS SP5 II were analyzed with
12 Leica LAS X software (Leica).

13 For vasculature layer imaging, cells were permeabilized with 0.5% Triton-X 100 for 30
14 min and then stained with Phalloidin 488 (1:50) (Molecular Probe A12379) and Hoechst nuclear
15 stain (1:1000) (Molecular Probe H1399) overnight. After overnight incubation, cells were rinsed
16 thrice with 0.2% Triton-X 100 for 10 min each and then covered with PBS for imaging. Devices
17 were placed on a 75 mm x 50 mm glass coverslip (#260462, Ted Pella Inc., Redding, CA, USA)
18 and placed in an Omnitray™ with a 45 mm x 70 mm rectangle cut out of the bottom. Fluorescent
19 images were obtained on a Zeiss Axiovert 200 coupled with an Axiocam 503 mono camera (Carl
20 Zeiss AG, Oberkochen, Germany). Images obtained were analyzed with Fiji (ImageJ).

21

22 *Angiogenesis Morphological Analysis:*

23 To analyze differences in morphology in the endothelial layer we used default functions
24 of Image J (Fiji) to quantify the tubule index (perimeter/area ratio)(Theberge et al. 2015a). The
25 image analysis procedure is described in the methods and SI of Theberge et al.(Theberge et al.
26 2015a), a summary is included here. For quantification, the 8-bit image containing the phalloidin
27 channel (488) was selected and a threshold (Huang Dark) was applied to get the outline of the
28 endothelial culture and saved (Image 1). The “Fill Holes” function was applied and saved (Image
29 2), and then Image 2 was subtracted from Image 1 to generate an image containing the
30 holes/gaps in the endothelial morphology (Image 3). The total area of the phalloidin stain was
31 then calculated by subtracting the area of Image 3 (holes) from Image 2 (fill holes), and the
32 perimeter of the stain was calculated by adding the perimeter of Image 2 and Image 3. The area
33 and perimeter were measured using the function “Analyze Particles”, with the following
34 parameters: size: 25-infinity (include pixel units), circularity: 0.00-1.00. The ImageJ macro for
35 this process is included in the supplementary materials and is based off the macro used in Yu et
36 al.(Yu et al. 2019)

37 Exclusion criteria for experimental artifacts that interfered with the imaging technique
38 was developed to exclude wells unable to be analyzed with this technique. For example, if a
39 collagen plug from the model granuloma layer detached and fell into a endothelial layer well
40 during separation of the layers, the endothelial morphology was obscured by signal from the
41 MDMs in the collagen plug and therefore unable to be accurately measured. All images were
42 assigned a randomized code and individuals not involved in the project determined which images

1 to exclude base on established criteria. Images were then analyzed according to the measurement
2 protocol above.

3 4 *Cytokine Analysis:*

5 Cytokine analyses were performed with a custom Luminex ProcartaPlex multiplex assay
6 for IL-6, TNF α , and VEGF (ThermoFisher). Supernatant samples were collected and pooled
7 from a single device (n=24 wells, 8 μ L/well) during daily media changes and stored at -80°C
8 until use. Samples were collected from the same device over a five-day period, such that each
9 sample contains cytokines secreted within 24 h of collection (i.e., Day 2 p.i. cytokine levels
10 indicate what was secreted between Day 1 and Day 2 p.i., etc.). For analysis, samples were
11 thawed on ice and analyzed according to the manufacturer's protocols for Luminex multiplex
12 assays. Samples were analyzed on a Luminex 100/200 System instrument with xPONENT
13 software (Fred Hutchinson Cancer Center Core Facility). All results were analyzed and
14 visualized using Prism 7 software (GraphPad Software, San Diego, CA, USA).

15 16 **Acknowledgements:**

17 We would like to thank Dr. Shahin Shafiani (Urdahl Lab) for providing the mCherry *M.*
18 *bovis* BCG strain, Dr. Jason Yu for providing help on the Stacks platform, Tammi van Neel and
19 Tianzi Zhang for image review, Ashley Dostie for obtaining the Stacks image, and Erik Layton
20 (Seshadri Lab) for PBMC isolation training. We acknowledge the support of the Biochemical
21 Diagnostics Foundry for Translational Research supported by the MJ Murdock Trust. This work
22 was supported by NIH R35GM128648, the University of Washington, the Mary Gates
23 Endowment, and by the National Science Foundation Graduate Research Fellowship Program
24 under Grant No. DGE-1256082 (SBB). Any opinions, findings, and conclusions or
25 recommendations expressed in this material are those of the author(s) and do not necessarily
26 reflect the views of the National Science Foundation.

27 28 **Conflicts of Interest:**

29 The authors acknowledge the following potential conflicts of interest in companies
30 pursuing open microfluidic technologies: ABT: Stacks to the Future, LLC.

31 32 **Author Contributions:**

33 SBB and ABT conceived of the project. SBB and MSG performed all experiments and
34 data analysis. SBB and MSG wrote the manuscript, and XS, CS, and ABT advised the project
35 and edited, revised, and provided feedback on the manuscript. All authors reviewed and
36 approved the final manuscript.

37 38 **References:**

39 Berry, Matthew P.R., Christine M. Graham, Finlay W. McNab, Zhaohui Xu, Susannah A.A.
40 Bloch, Tolu Oni, Katalin A. Wilkinson, et al. 2010. "An Interferon-Inducible Neutrophil-
41 Driven Blood Transcriptional Signature in Human Tuberculosis." *Nature* 466 (7309): 973–
42 77. <https://doi.org/10.1038/nature09247>.
43 Berthier, Erwin, Ashley M. Dostie, Ulri N. Lee, Jean Berthier, and Ashleigh B. Theberge. 2019.

- 1 “Open Microfluidic Capillary Systems.” *Analytical Chemistry* 91 (14): 8739–50.
2 <https://doi.org/10.1021/acs.analchem.9b01429>.
- 3 Bielecka, Magdalena K., Liku B. Tezera, Robert Zmijan, Francis Drobniewski, Xunli Zhang,
4 Suwan Jayasinghe, and Paul Elkington. 2017. “A Bioengineered Three-Dimensional Cell
5 Culture Platform Integrated with Microfluidics to Address Antimicrobial Resistance in
6 Tuberculosis.” *MBio* 8 (1). <https://doi.org/10.1128/mBio.02073-16>.
- 7 Birkness, Kristin A., Jeannette Guarner, Suraj B. Sable, Ralph A. Tripp, Kathryn L. Kellar,
8 Jeanine Bartlett, and Frederick D. Quinn. 2007. “An in Vitro Model of the Leukocyte
9 Interactions Associated with Granuloma Formation in Mycobacterium Tuberculosis
10 Infection.” *Immunology and Cell Biology* 85 (2): 160–68.
11 <https://doi.org/10.1038/sj.icb.7100019>.
- 12 Bishop, Eileen T., Graham T. Bell, Stephen Bloor, I. J. Broom, Neil F.K. Hendry, and Denys N.
13 Wheatley. 1999. “An in Vitro Model of Angiogenesis: Basic Features.” *Angiogenesis* 3 (4):
14 335–44. <https://doi.org/10.1023/A:1026546219962>.
- 15 Casavant, Benjamin P., Erwin Berthier, Ashleigh B Theberge, Jean Berthier, Sara I Montanez-
16 Sauri, Lauren L Bischel, Kenneth Brakke, et al. 2013. “Suspended Microfluidics.” *PNAS*
17 110 (25): 10111–16. <https://doi.org/10.1073/pnas.1302566110>.
- 18 Cronan, Mark R., Molly A. Matty, Allison F. Rosenberg, Landry Blanc, Charlie J. Pyle, Scott T.
19 Espenschied, John F. Rawls, Véronique Dartois, and David M. Tobin. 2018. “An Explant
20 Technique for High-Resolution Imaging and Manipulation of Mycobacterial Granulomas.”
21 *Nature Methods* 15 (12): 1098–1107. <https://doi.org/10.1038/s41592-018-0215-8>.
- 22 Cronan, Mark R., and David M. Tobin. 2014. “Fit for Consumption: Zebrafish as a Model for
23 Tuberculosis.” *DMM Disease Models and Mechanisms* 7 (7): 777–84.
24 <https://doi.org/10.1242/dmm.016089>.
- 25 Crouser, Elliott D., Peter White, Evelyn Guirado Caceres, Mark W. Julian, Audrey C. Papp,
26 Landon W. Locke, Wolfgang Sadee, and Larry S. Schlesinger. 2017. “A Novel in Vitro
27 Human Granuloma Model of Sarcoidosis and Latent Tuberculosis Infection.” *American*
28 *Journal of Respiratory Cell and Molecular Biology* 57 (4): 487–98.
29 <https://doi.org/10.1165/rcmb.2016-0321OC>.
- 30 Darboe, Fatoumatta, Stanley Kimbung Mbandi, Kogieleum Naidoo, Nonhlanhla Yende-Zuma,
31 Lara Lewis, Ethan G. Thompson, Fergal J. Duffy, et al. 2019. “Detection of Tuberculosis
32 Recurrence, Diagnosis and Treatment Response by a Blood Transcriptomic Risk Signature
33 in HIV-Infected Persons on Antiretroviral Therapy.” *Frontiers in Microbiology* 10 (JUN):
34 1–16. <https://doi.org/10.3389/fmicb.2019.01441>.
- 35 Datta, Meenal, Laura E. Via, Walid S. Kamoun, Chong Liu, Wei Chen, Giorgio Seano, Danielle
36 M. Weiner, et al. 2015. “Anti-Vascular Endothelial Growth Factor Treatment Normalizes
37 Tuberculosis Granuloma Vasculature and Improves Small Molecule Delivery.” *Proceedings*
38 *of the National Academy of Sciences of the United States of America* 112 (6): 1827–32.
39 <https://doi.org/10.1073/pnas.1424563112>.
- 40 Deb, Chirajyoti, Chang Muk Lee, Vinod S. Dubey, Jaiyanth Daniel, Bassam Abomoelak, Tatiana
41 D. Sirakova, Santosh Pawar, Linda Rogers, and Pappachan E. Kolattukudy. 2009. “A Novel

- 1 in Vitro Multiple-Stress Dormancy Model for Mycobacterium Tuberculosis Generates a
2 Lipid-Loaded, Drug-Tolerant, Dormant Pathogen.” *PLoS ONE* 4 (6).
3 <https://doi.org/10.1371/journal.pone.0006077>.
- 4 Domingo-Gonzalez, Racquel, Oliver Prince, Andrea Cooper, and Shabaana A. Khader. 2016.
5 “Cytokines and Chemokines in Mycobacterium Tuberculosis Infection.” *Microbiology*
6 *Spectrum* 4 (5): 1–37. <https://doi.org/10.1128/microbiolspec.tbtb2-0018-2016>.
- 7 Elkington, Paul, Maria Lerm, Nidhi Kapoor, Robert Mahon, Elsje Pienaar, Dongeun Huh,
8 Deepak Kaushal, and Larry S. Schlesinger. 2019. “In Vitro Granuloma Models of
9 Tuberculosis: Potential and Challenges.” *Journal of Infectious Diseases* 219 (12): 1858–66.
10 <https://doi.org/10.1093/infdis/jiz020>.
- 11 Engele, Matthias, Elmar Stöbel, Kirstin Castiglione, Nives Schwerdtner, Manfred Wagner, Pal
12 Bölcskei, Martin Röllinghoff, and Steffen Stenger. 2002. “Induction of TNF in Human
13 Alveolar Macrophages As a Potential Evasion Mechanism of Virulent Mycobacterium
14 Tuberculosis.” *The Journal of Immunology* 168 (3): 1328–37.
15 <https://doi.org/10.4049/jimmunol.168.3.1328>.
- 16 Foreman, Taylor W., Smriti Mehra, Andrew A. Lackner, and Deepak Kaushal. 2017.
17 “Translational Research in the Nonhuman Primate Model of Tuberculosis.” *ILAR Journal*
18 58 (2): 151–59. <https://doi.org/10.1093/ilar/ilx015>.
- 19 Gern, B., C. Plumlee, M. Gerner, and K. Urdahl. 2017. “Investigating Immune Correlates of
20 Protection to Tuberculosis Using an Ultra-Low Dose Infection in a Mouse Model.” *OFID* 4
21 (Suppl 1): 47–48.
- 22 Guyot-Revol, Valerie, John A. Innes, Sarah Hackforth, Tim Hinks, and Ajit Lalvani. 2006.
23 “Regulatory T Cells Are Expanded in Blood and Disease Sites in Patients with
24 Tuberculosis.” *American Journal of Respiratory and Critical Care Medicine* 173 (7): 803–
25 10. <https://doi.org/10.1164/rccm.200508-1294OC>.
- 26 Harding, Jeffrey S., Melinda Herbath, Yuli Chen, Aditya Rayasam, Anna Ritter, Balazs Csoka,
27 George Hasko, et al. 2019. “VEGF-A from Granuloma Macrophages Regulates
28 Granulomatous Inflammation by a Non-Angiogenic Pathway during Mycobacterial
29 Infection.” *Cell Reports* 27 (7): 2119–2131.e6. <https://doi.org/10.1016/j.celrep.2019.04.072>.
- 30 Humayun, Mouhita, Chung Wai Chow, and Edmond W.K. Young. 2018. “Microfluidic Lung
31 Airway-on-a-Chip with Arrayable Suspended Gels for Studying Epithelial and Smooth
32 Muscle Cell Interactions.” *Lab on a Chip* 18 (9): 1298–1309.
33 <https://doi.org/10.1039/c7lc01357d>.
- 34 Kapoor, Nidhi, Santosh Pawar, Tatiana D. Sirakova, Chirajyoti Deb, William L. Warren, and
35 Pappachan E. Kolattukudy. 2013. “Human Granuloma In Vitro Model, for TB Dormancy
36 and Resuscitation.” *PLoS ONE* 8 (1). <https://doi.org/10.1371/journal.pone.0053657>.
- 37 Kaufmann, S. H.E. 2004. “New Issues in Tuberculosis.” *Annals of the Rheumatic Diseases* 63
38 (SUPPL. 2): 50–56. <https://doi.org/10.1136/ard.2004.028258>.
- 39 Koh, Wonshill, Amber N. Stratman, Anastasia Sacharidou, and George E. Davis. 2008. “Chapter
40 5 In Vitro Three Dimensional Collagen Matrix Models of Endothelial Lumen Formation

- 1 During Vasculogenesis and Angiogenesis.” *Methods in Enzymology* 443 (08): 83–101.
2 [https://doi.org/10.1016/S0076-6879\(08\)02005-3](https://doi.org/10.1016/S0076-6879(08)02005-3).
- 3 Lin, Philana Ling, Hillarie L. Plessner, Nikolai N. Voitenok, and Jo Anne L. Flynn. 2007.
4 “Tumor Necrosis Factor and Tuberculosis.” *Journal of Investigative Dermatology*
5 *Symposium Proceedings* 12 (1): 22–25. <https://doi.org/10.1038/sj.jidsymp.5650027>.
- 6 Lonza. 2018. “Clonetics Endothelial Cell System Technical Information & Instructions,” 1–15.
7 https://bioscience.lonza.com/lonza_bs/US/en/download/product/asset/29423.
- 8 Martinez, Alejandra N., Smriti Mehra, and Deepak Kaushal. 2013. “Role of Interleukin 6 in
9 Innate Immunity to Mycobacterium Tuberculosis Infection.” *Journal of Infectious Diseases*
10 207 (8): 1253–61. <https://doi.org/10.1093/infdis/jit037>.
- 11 Myllymäki, Henna, Carina A. Bäuerlein, and Mika Rämet. 2016. “The Zebrafish Breathes New
12 Life into the Study of Tuberculosis.” *Frontiers in Immunology* 7 (MAY).
13 <https://doi.org/10.3389/fimmu.2016.00196>.
- 14 Oehlers, Stefan H., Mark R. Cronan, Rebecca W. Beerman, Matthew G. Johnson, Jianhua
15 Huang, Christopher D. Kontos, Jason E. Stout, and David M. Tobin. 2017. “Infection-
16 Induced Vascular Permeability Aids Mycobacterial Growth.” *Journal of Infectious Diseases*
17 215 (5): 813–17. <https://doi.org/10.1093/infdis/jiw355>.
- 18 Oehlers, Stefan H., Mark R. Cronan, Ninecia R. Scott, Monica I. Thomas, Kazuhide S. Okuda,
19 Eric M. Walton, Rebecca W. Beerman, Philip S. Crosier, and David M. Tobin. 2015.
20 “Interception of Host Angiogenic Signalling Limits Mycobacterial Growth.” *Nature* 517
21 (7536): 612–15. <https://doi.org/10.1038/nature13967>.
- 22 Ogongo, Paul, Adrie J.C. Steyn, Farina Karim, Kaylesh J. Dullabh, Ismael Awala, Rajhmun
23 Madansein, Alasdair Leslie, and Samuel M. Behar. 2020. “Differential Skewing of Donor-
24 Unrestricted and $\Gamma\delta$ T Cell Repertoires in Tuberculosis-Infected Human Lungs.” *Journal of*
25 *Clinical Investigation* 130 (1): 214–30. <https://doi.org/10.1172/JCI130711>.
- 26 Ong, Louis Jun Ye, Terry Ching, Lor Huai Chong, Seep Arora, Huan Li, Michinao Hashimoto,
27 Ramanuj Dasgupta, Po Ki Yuen, and Yi Chin Toh. 2019. “Self-Aligning Tetris-Like (TILE)
28 Modular Microfluidic Platform for Mimicking Multi-Organ Interactions.” *Lab on a Chip* 19
29 (13): 2178–91. <https://doi.org/10.1039/c9lc00160c>.
- 30 Oshero, Nir, and Ronen Ben-Ami. 2016. “Modulation of Host Angiogenesis as a Microbial
31 Survival Strategy and Therapeutic Target.” *PLoS Pathogens*.
32 <https://doi.org/10.1371/journal.ppat.1005479>.
- 33 Parasa, Venkata R., Jagadeeswara R. Muvva, Jeronimo F. Rose, Clara Braian, Susanna
34 Brighenti, and Maria Lerm. 2017. “Inhibition of Tissue Matrix Metalloproteinases
35 Interferes with Mycobacterium Tuberculosis-Induced Granuloma Formation and Reduces
36 Bacterial Load in a Human Lung Tissue Model.” *Frontiers in Microbiology* 8 (DEC): 1–14.
37 <https://doi.org/10.3389/fmicb.2017.02370>.
- 38 Parasa, Venkata Ramanarao, Muhammad Jubayer Rahman, Anh Thu Ngyuen Hoang, Mattias
39 Svensson, Susanna Brighenti, and Maria Lerm. 2014. “Modeling Mycobacterium
40 Tuberculosis Early Granuloma Formation in Experimental Human Lung Tissue.” *DMM*

- 1 *Disease Models and Mechanisms* 7 (2): 281–88. <https://doi.org/10.1242/dmm.013854>.
- 2 Peyron, Pascale, Julien Vaubourgeix, Yannick Poquet, Florence Levillain, Catherine Botanch,
3 Fabienne Bardou, Mamadou Daffé, et al. 2008. “Foamy Macrophages from Tuberculous
4 Patients’ Granulomas Constitute a Nutrient-Rich Reservoir for M. Tuberculosis
5 Persistence.” *PLoS Pathogens* 4 (11): 1–14. <https://doi.org/10.1371/journal.ppat.1000204>.
- 6 Polena, Helena, Frédéric Boudou, Sylvain Tilleul, Nicolas Dubois-Colas, Cécile Lecointe,
7 Niaina Rakotosamimanana, Mattia Pelizzola, et al. 2016. “Mycobacterium Tuberculosis
8 Exploits the Formation of New Blood Vessels for Its Dissemination.” *Scientific Reports* 6
9 (August): 1–11. <https://doi.org/10.1038/srep33162>.
- 10 Puissegur, Marie Pierre, Catherine Botanch, Jean Luc Duteyrat, Georges Delsol, Claude
11 Caratero, and Frédéric Altare. 2004. “An in Vitro Dual Model of Mycobacterial
12 Granulomas to Investigate the Molecular Interactions between Mycobacteria and Human
13 Host Cells.” *Cellular Microbiology* 6 (5): 423–33. [https://doi.org/10.1111/j.1462-
14 5822.2004.00371.x](https://doi.org/10.1111/j.1462-5822.2004.00371.x).
- 15 Ramakrishnan, Lalita. 2012. “Revisiting the Role of the Granuloma in Tuberculosis.” *Nature
16 Reviews Immunology* 12 (5): 352–66. <https://doi.org/10.1038/nri3211>.
- 17 Russell, David G., Pere Joan Cardona, Mi Jeong Kim, Sophie Allain, and Frédéric Altare. 2009.
18 “Foamy Macrophages and the Progression of the Human Tuberculosis Granuloma.” *Nature
19 Immunology* 10 (9): 943–48. <https://doi.org/10.1038/ni.1781>.
- 20 Sarkanen, Jertta Riina, Marika Mannerström, Hanna Vuorenää, Jukka Uotila, Timo Ylikomi,
21 and Tuula Heinonen. 2011. “Intra-Laboratory Pre-Validation of a Human Cell Based in
22 Vitro Angiogenesis Assay for Testing Angiogenesis Modulators.” *Frontiers in
23 Pharmacology* JAN (January): 1–13. <https://doi.org/10.3389/fphar.2010.00147>.
- 24 Saunders, Bernadette M., and Warwick J. Britton. 2007. “Life and Death in the Granuloma:
25 Immunopathology of Tuberculosis.” *Immunology and Cell Biology* 85 (2): 103–11.
26 <https://doi.org/10.1038/sj.icb.7100027>.
- 27 Scanga, Charles A., and Joanne L. Flynn. 2014. “Modeling Tuberculosis in Nonhuman
28 Primates.” *Cold Spring Harbor Perspectives in Medicine* 4 (12).
29 <https://doi.org/10.1101/cshperspect.a018564>.
- 30 Seitzer, Ulrike, and Johannes Gerdes. 2003. “Generation and Characterization of Multicellular
31 Heterospheroids Formed by Human Peripheral Blood Mononuclear Cells.” *Cells Tissues
32 Organs* 174 (3): 110–16. <https://doi.org/10.1159/000071151>.
- 33 Singh, Prati Pal, and Amit Goyal. 2013. “Interleukin-6: A Potent Biomarker of Mycobacterial
34 Infection.” *SpringerPlus* 2 (1): 2–9. <https://doi.org/10.1186/2193-1801-2-686>.
- 35 Su, Xiaojing, Ashleigh B. Theberge, Craig T. January, and David J. Beebe. 2013. “Effect of
36 Microculture on Cell Metabolism and Biochemistry: Do Cells Get Stressed in
37 Microchannels?” *Analytical Chemistry* 85 (3): 1562–70. <https://doi.org/10.1021/ac3027228>.
- 38 Tezera, Liku B., Magdalena K. Bielecka, Andrew Chancellor, Michaela T. Reichmann, Basim Al
39 Shammari, Patience Brace, Alex Batty, et al. 2017. “Dissection of the Host-Pathogen
40 Interaction in Human Tuberculosis Using a Bioengineered 3-Dimensional Model.” *ELife* 6:

- 1 1–19. <https://doi.org/10.7554/eLife.21283>.
- 2 Theberge, Ashleigh B., Jiaquan Yu, Edmond W.K. Young, William A. Ricke, Wade Bushman,
3 and David J. Beebe. 2015a. “Microfluidic Multiculture Assay to Analyze Biomolecular
4 Signaling in Angiogenesis.” *Analytical Chemistry* 87 (6): 3239–46.
5 <https://doi.org/10.1021/ac503700f>.
- 6 Theberge, Ashleigh B., Jiaquan Yu, Edmond W K Young, William A. Ricke, Wade Bushman,
7 and David J. Beebe. 2015b. “Microfluidic Multiculture Assay to Analyze Biomolecular
8 Signaling in Angiogenesis.” *Analytical Chemistry*. <https://doi.org/10.1021/ac503700f>.
- 9 Torraca, Vincenzo, Claudia Tulotta, B. Ewa Snaar-Jagalska, and Annemarie H. Meijer. 2017.
10 “The Chemokine Receptor CXCR4 Promotes Granuloma Formation by Sustaining a
11 Mycobacteria-Induced Angiogenesis Programme.” *Scientific Reports* 7 (February): 18–20.
12 <https://doi.org/10.1038/srep45061>.
- 13 World Health Organization. 2019. “Global Tuberculosis Report 2019.”
- 14 Yong, Kylie Su Mei, Zhisheng Her, and Qingfeng Chen. 2018. “Humanized Mice as Unique
15 Tools for Human-Specific Studies.” *Archivum Immunologiae et Therapiae Experimentalis*
16 66 (4): 245–66. <https://doi.org/10.1007/s00005-018-0506-x>.
- 17 Yu, Jiaquan, Erwin Berthier, Alexandria Craig, Theodorus E. de Groot, Sidney Sparks, Patrick
18 N. Ingram, David F. Jarrard, Wei Huang, David J. Beebe, and Ashleigh B. Theberge. 2019.
19 “Reconfigurable Open Microfluidics for Studying the Spatiotemporal Dynamics of
20 Paracrine Signalling.” *Nature Biomedical Engineering* 3 (10): 830–41.
21 <https://doi.org/10.1038/s41551-019-0421-4>.
- 22 Zhan, Lingjun, Jun Tang, Mengmeng Sun, and Chuan Qin. 2017. “Animal Models for
23 Tuberculosis in Translational and Precision Medicine.” *Frontiers in Microbiology* 8
24 (MAY). <https://doi.org/10.3389/fmicb.2017.00717>.
- 25